Ishaq, H.; Dincer, Ibrahim

Article

A new energy system based on biomass gasification for hydrogen and power production

Energy Reports

Provided in Cooperation with:
Elsevier

Suggested Citation: Ishaq, H.; Dincer, Ibrahim (2020) : A new energy system based on biomass gasification for hydrogen and power production, Energy Reports, ISSN 2352-4847, Elsevier, Amsterdam, Vol. 6, pp. 771-781, https://doi.org/10.1016/j.egyr.2020.02.019

Energy Reports 6 (2020) 771–781

Contents lists available at ScienceDirect

Energy Reports

journal homepage: www.elsevier.com/locate/egyr

Research paper

A new energy system based on biomass gasification for hydrogen and power production

H. Ishaq *, I. Dincer

Clean Energy Research Laboratory, Faculty of Engineering and Applied Science, University of Ontario Institute of Technology, 2000 Simcoe Street North, Oshawa, Ontario, L1H 7K4, Canada

ARTICLE INFO

Article history:
Received 22 June 2019
Received in revised form 14 December 2019
Accepted 24 February 2020
Available online xxxx

Keywords:
Biomass gasification
Hydrogen production
PEM electrolyzer
Cryogenic air separation unit
Power production
Efficiency

ABSTRACT

In this paper, a new gasification system is developed for the three useful outputs of electricity, heat and hydrogen and reported for practical energy applications. The study also investigates the composition of syngas leaving biomass gasifier. The composition of syngas is represented by the fractions of hydrogen, carbon dioxide, carbon monoxide and water. The integrated energy system comprises of an entrained flow gasifier, a Cryogenic Air Separation (CAS) unit, a double-stage Rankine cycle, Water Gas Shift Reactor (WGSR), a combined gas–steam power cycle and a Proton Exchange Membrane (PEM) electrolyzer. The whole integrated system is modeled in the Aspen plus 9.0 excluding the PEM electrolyzer which is modeled in Engineering Equation Solver (EES). A comprehensive parametric investigation is conducted by varying numerous parameters like biomass flow rate, steam flow rate, air input flow rate, combustion reactor temperature, and power supplied to the electrolyzer. The system is designed in a way to supply the power produced by the steam Rankine cycle to the PEM electrolyzer for hydrogen production. The overall energy efficiency is obtained to be 53.7% where the exergy efficiency is found to be 45.5%. Furthermore, the effect of the biomass flow rate is investigated on the various system operational parameters.

1. Introduction

Coal is the utmost abundant fossil fuel type on earth. Nevertheless, utilizing and burning fossil fuel results into significant environmental impact (Muradov and Veziroğlu, 2008). However, the most prevailing fossil fuel on the globe is coal and the increase in the coal demand is leading to the incredible carbon emissions and global warming (Ozturk, 2017). Currently, with the rise in carbon emission, numerous investigations are focusing on renewable energy sources, like solar, wind, hydro and biomass (Turner et al., 2008; Ishaq and Dincer, 2019). New studies are dedicating more research and devotion to produce hydrogen and electricity from biomass because environmentally, biomass is advantageous and has fewer carbon emissions as compared to the coal (Gunarathne et al., 2016; Dimpl, 2011; Roddy and Manson-Whitton, 2012; Basu and Francisco, 2010).

Andersson and Lundgren (2014) presented a study on ammonia production by producing nitrogen and hydrogen. A more environmentally benign method, hydrogen production by lignocellulosic biomass gasification was utilized in this paper. An economic analysis was conducted in this study on ammonia production based on the biomass gasification. This study concluded that according to the economic analysis and performance analysis, the designed methodology was favorable. Uzi et al. (2019) focused on the pyrolysis and gasification of woody biomass and performed experimental investigation to analyze chemical characterization. Sikarwar et al. (2016) presented a comprehensive review study on the advancements in biomass gasification. This study also presented a strategy to improve the sustainability and feasibility of biomass gasification via technological advancement and minimization the environmental effects.

Islam et al. (2017) analyzed two different biomass based energy systems with a thermoelectric generator. The designed system consisted of biomass gasification, organic Rankine cycles, absorption chillers, thermoelectric generator and electrolysis. A part of the power produced by the thermoelectric generators by employed to the electrolysis for hydrogen production. The energy efficiencies of the two designed systems were finalized accordingly as 73.4% and 74.5% while the exergy efficiencies were found to be 33.3% and 34.02% respectively. Safari et al. (2016) investigated a co-generation system for power and hydrogen production by sugarcane bagasse via supercritical water gasification. For the proposed system, Aspen plus was employed to conduct thermodynamic equilibrium model. The investigations of the temperature effect on the designed system resulted that it has direct relation with hydrogen production and higher temperature

* Corresponding author.
E-mail address: haris.ishaq@uoit.net (H. Ishaq).

https://doi.org/10.1016/j.egyr.2020.02.019

is favored. The modeled system provided 56 kW of power and 8.55 kg/h of hydrogen production.

Gunarathne et al. (2016) conducted a performance assessment of a biomass and heat recovery based integrated system. Heat treatment was considered for the steel industrial furnace. The challenges found for utilizing renewable sources in steel industry were not only related to the carbon emissions but also the system efficiency. Multi-stage gasification system was integrated in this paper with heat treatment furnace. In this study, five different cases were studied and their performance was investigated in many aspects like heat demand, biomass input and the system efficiency. Khalid et al. (2015) developed a biomass–solar hybrid multi-generation system for the useful products of electricity, hot water, cooling and heated air. The chemical composition of the biomass used during the analysis was provided in the paper and used for the energy and exergy analyses. Numerous variables, namely reference temperature, aperture area of the solar heliostat and the direct normal irradiation were considered to investigate the system performance and the effect of these parameters was also studied on the system efficiencies.

Abuadala et al. (2009) conducted an exergy analysis of a biomass based energy system. The hydrogen production achieved by the proposed biomass based energy system was in the range of 10–32 kg/s. In the designed system, biomass was directly introduced in the gasification reactor at operating conditions like temperature of 1000–1500 K and the steam was entered at a temperature of 500 K with a flow rate of 4.5 kg/s. The study predicted that the two factors which can improve hydrogen production are steam amount and biomass quality. Ellis et al. (2015) conducted a study on the biomass and coal gasification and investigated the mineral matter interactions.

A novel biomass based energy system is proposed in this study for the useful commodities of hydrogen, power and heating. Modeling and the performance measures are conducted for the proposed system on the basis of energy and exergy analysis. The explicit objectives of this study are (i) to configure a new biomass energy based integrated system, (ii) the entire system is modeled and simulated using Aspen plus and the model equations for each unit are described (iii) to investigate the novel configuration for multigeneration purpose and achieving high energetic and exergetic efficiencies. Furthermore, the study aims to produce power, heating and hydrogen in a competent manner as included performance investigation.

2. System description

The proposed energy system utilizes biomass renewable energy source and integrated with different subsystems. The major subsystems are cryogenic air separation (CAS), a double-stage Rankine cycle, a combined Brayton cycle and a proton exchange membrane (PEM) electrolyzer. Fig. 1 shows the schematic layout of the proposed energy system while Fig. 2 gives the Aspen plus simulation layout of the designed energy system. The entrained flow gasifier is employed for the syngas production utilizing the biomass and steam is utilized as the gasification agent and the gasification model is based on this study (Al-Zareer et al., 2018a). The design parameters of the modeled system are arranged in Table 1. In order to provide gasifier with the required amount of oxygen, a CAS unit is placed within the same system.

The input air is compressed with the help of a compressor in order to achieve the operating pressure. Thus, with the help of a distillation column, oxygen is separated from the nitrogen. As both of these streams leave at high temperature and pressure, they are passed through a heat exchanger in order to recover the heat and provide is to the nitrogen stream. This stream further passes through a turbine to generate power and additional heat available is recovered for the combustion reactor. The oxygen stream is further compressed at a pressure of entrained flow gasifier to reach the same pressure. The distillation column in the CAS unit requires heat for the reboiler and some cooling is also required because of the condenser being at very low temperature. The chemical composition of the biomass utilized in this paper is provided in Table 2. The biomass gasification reactor is operated at temperature of 850 °C in order to achieve syngas with high grade and biomass composition balance in the reaction depends upon the chemical composition.

$$Biomass \rightarrow Char + (C_6H_6 + CO + H_2 + CO_2 + N_2 + CH_4 + H_2O + H_2S)$$

The volatile matter is included in the pyrolysis product and these volatile matters are combusted in pyrolysis. The reactions of volatile matter combustion, char decomposition, and chemical species decomposed from char are as follows:

$$H_2 + 0.5\ O_2 \rightarrow H_2O$$
$$CO + 0.5\ O_2 \rightarrow CO_2$$
$$CH_4 + 2O_2 \rightarrow 2H_2O + CO_2$$
$$C_6H_6 + 7.5\ O_2 \rightarrow 3H_2O + 6CO_2$$
$$char \rightarrow C + O_2 + N_2 + H_2 + S + Ash$$
$$C + O_2 \rightarrow CO_2$$
$$C + 0.5O_2 \rightarrow CO$$
$$CO + H_2O \rightarrow CO_2 + H_2$$
$$C + 2H_2 \rightarrow CH_4$$
$$C + CO_2 \rightarrow 2CO$$
$$CH_4 + H_2O \rightarrow CO_2 + H_2$$
$$C + H_2O \rightarrow CO + H_2$$
$$S + H_2 \rightarrow H_2S$$

The syngas is produced at very high temperature and pressure which passes through a turbine to generate power and then leads towards the heat exchanger. The heat exchanger is employed in order to utilize the heat available for more purposes. The syngas stream leaves the heat exchanger at the temperature required by the water gas shift reactor (WGSR) and remaining available heat is integrated with a double-stage Rankine cycle where high-pressure turbine (HPT) provides with a 1.37 MW of power output while the low-pressure turbine (LPT) generate 1.4 MW of power. The additional heat is the condenser is used for heating purpose. The WGSR is employed to convert the carbon monoxide into carbon dioxide and to produce hydrogen by getting it reacted with steam and the conversion rate of this reaction is 0.982. The produced hydrogen is separated with the help of a separator and remaining is fed to the combined gas–steam power cycle. Through a compressor, air reaches the combustion chamber of the Brayton cycle. The exit of the combustion chamber is connected with a gas turbine to yield electricity. The exhaust gas of the turbine passes through the heat exchanger which works as a boiler for the steam Rankine cycle combined with Brayton cycle. The WGSR is exothermic reaction and additional heat is recovered and provided to the combustion chamber which also helps to maintain the operating temperature of WSGR and it follows:

$$CO\ (g) + H_2O\ (g) \rightarrow CO_2\ (g) + H_2\ (g)$$

The steam is used as a working fluid in the Rankine cycle combined with the Brayton cycle and the electricity produced by the steam turbine is fed to the PEM electrolyzer in order to produce hydrogen. The water is fed to the PEM electrolyzer with electric power which produces hydrogen for the storage purpose. The electric power generated by other subsystems is fed to the community as a useful commodity.

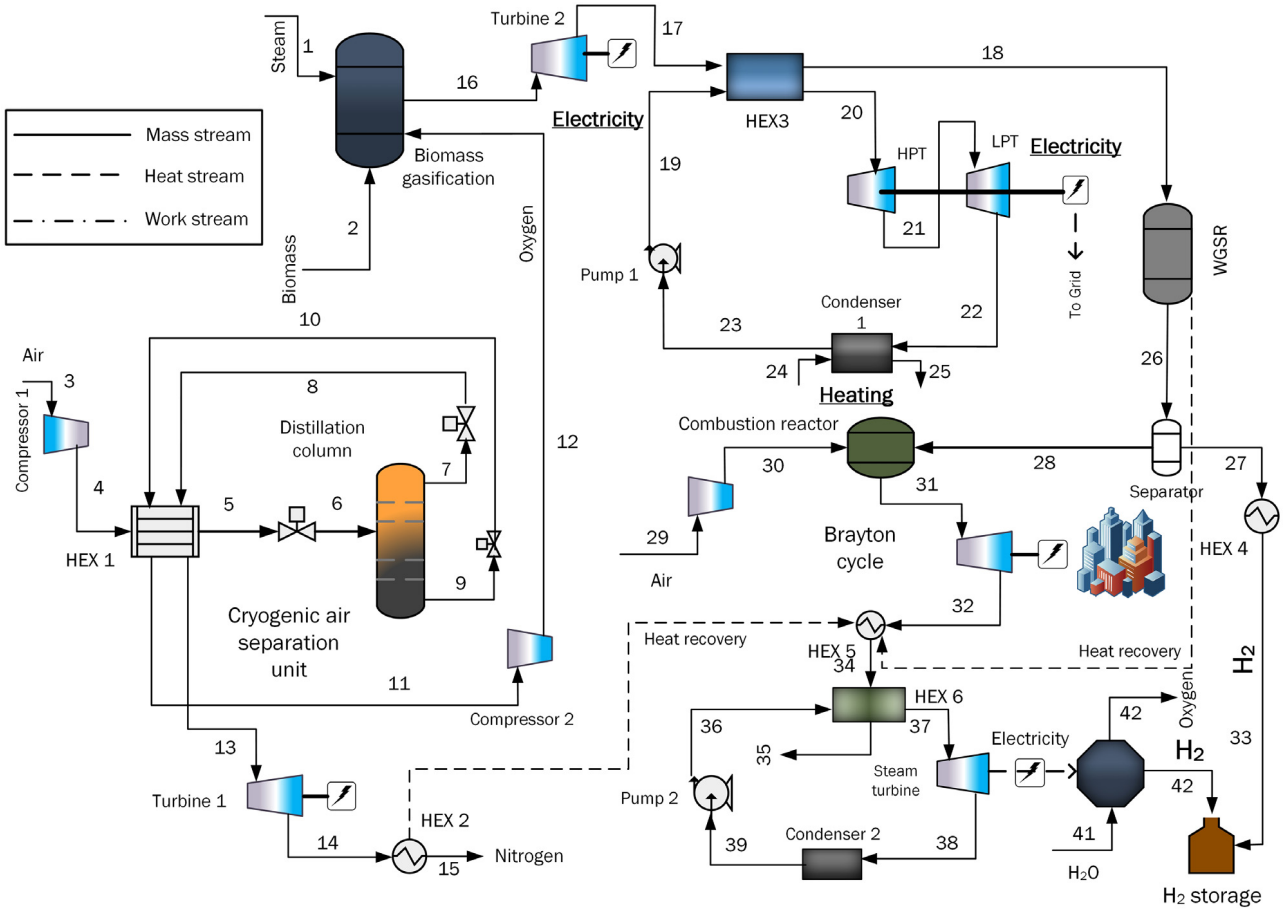

Fig. 1. Schematic flowsheet of the proposed energy system based on biomass gasification.

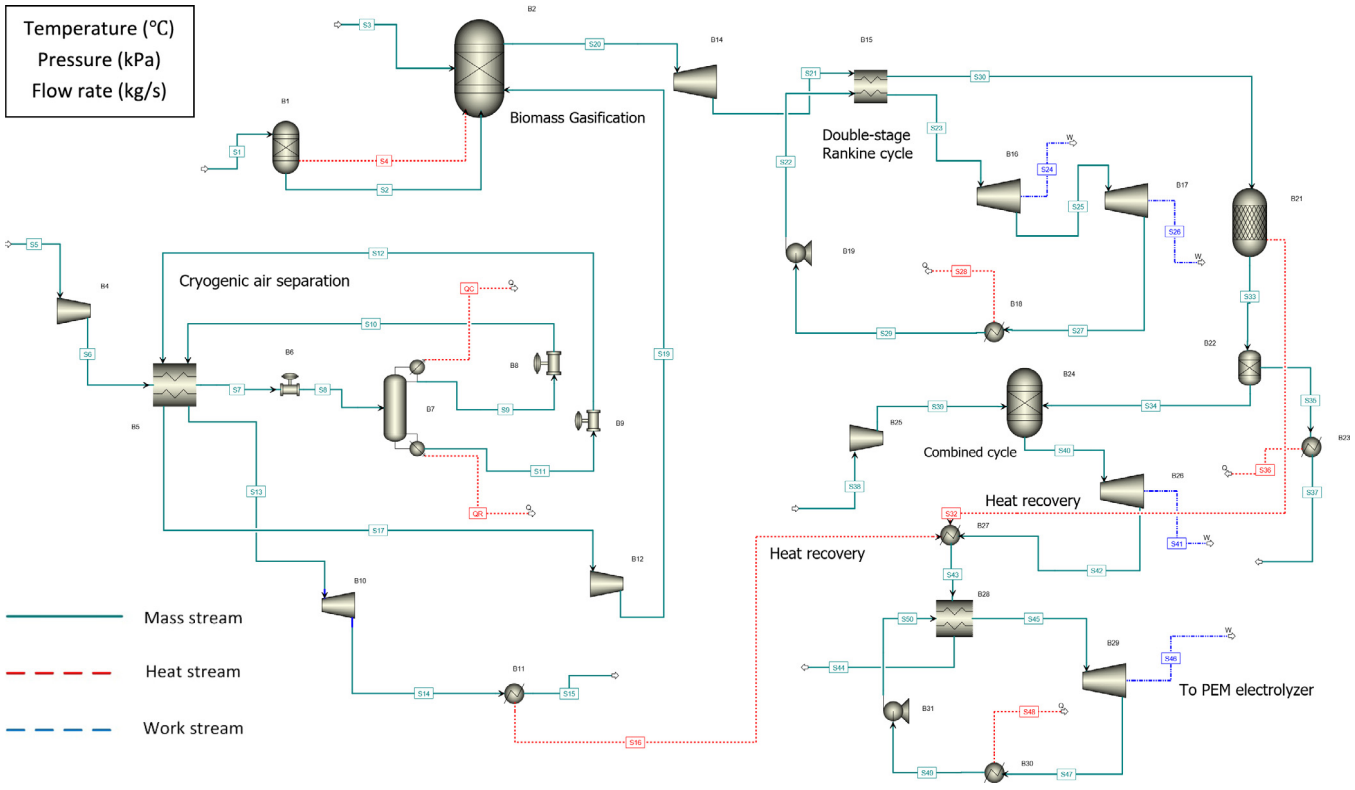

Fig. 2. Aspen plus simulation of the proposed energy system based on biomass gasification.

Table 1
Design parameters of the operating system.

System	Operating parameter	Value
Cryogenic air separation unit	Distillation column operating pressure	5 bar
	Air compressor pressure (Van der Ham and Kjelstrup, 2010)	8 bar
	Hydrogen and nitrogen output pressure from CAS unit	1.5 bar
Biomass gasifier	Biomass flow rate	0.4 kg/s
	Steam temperature	420 °C
	Entrained flow gasified pressure (Al-Zareer et al., 2018a)	24 bar
	Oxygen inlet temperature of the gasifier	484 °C
Double-stage Rankine cycle	High-pressure turbine discharge pressure (Al-Zareer et al., 2018a)	5 bar
	Low-pressure turbine discharge pressure	0.1 bar
Water gas shift reactor	Operating temperature (Augustine et al., 2011)	450 °C
	Operating pressure (Augustine et al., 2011)	14.4 bar
	Conversion rate	98.2%
Brayton cycle	Operating pressure of combustion chamber (Atif and Al-Sulaiman, 2018)	23 bar
	Operating pressure	500 °C
	Gas turbine discharge pressure	1.2 bar
Steam Rankine cycle	Steam turbine discharge pressure (Cengel and Boles, 2015)	0.1 bar
	Condenser temperature	30 °C
PEM electrolyzer	Faraday's constant	96 486 C/mol
	Temperature	80 °C
	Membrane thickness (Carmo et al., 2013)	0.1 mm
	Cathode pre-exponential factor j_c^{ref}	4.6×10^3 Am^{-2}
	Anode pre-exponential factor j_a^{ref}	1.7×10^5 Am^{-2}

Table 2
Biomass composition considered for the designed system.

Composition	Value
Biomass type	Dry Olive pits (dry basis by weight %)
Air to fuel ratio	5.75
C	48.81
N	0.36
H	6.23
S	0.02
O	43.48

3. Analysis

The proposed system is analyzed energetically and exergetically. The input design parameters considered during the system modeling and simulation are arranged in Table 1. The energy and exergy analyses are conducted on each single component in order to investigate the exergy destruction rates. All the gases are treated as ideal gases with a compressibility factor of 1, and reference temperature and pressure are assumed to be 25 °C and 1 atm, respectively. The proposed system is then simulated in Aspen Plus and EES software packages. The electric power, hydrogen and heating are the major useful commodities of the system.

As explained in Fig. 1, the biomass gasification is integrated with the energy system to produce syngas. The subscripts, blocks and stream names refers to the Aspen Plus schematic presented in Fig. 2. The state point results of each stream are arranged in Table 3.

The factors ex_{ph} and ex_{ch} represents the physical and chemical exergy and the correlations are expressed in the following equations:

$$ex_{ph} = h - h_0 - T_0(s - s_0) \tag{1}$$

$$ex_{ch} = \sum x_j ex_{ch}^0 + RT_0 \sum x_j \ln(x_j) \tag{2}$$

3.1. Biomass gasification

The expression used to determine the chemical exergy of the biomass is described in the following expression (Yan et al., 2015):

$$ex_{ch}^f = [(LHV + \omega h_{fg}) \times \beta + 9.417S] \tag{3}$$

The LHV is completely dependent on the chemical composition of the biomass and expression for calculating β can be expressed as:

$$\beta = 0.1882\frac{H}{C} + 0.061\frac{O}{C} + 0.0404\frac{N}{C} + 1.0437 \tag{4}$$

Here, H denotes hydrogen, O signifies oxygen, N presents nitrogen, and C denotes for oxygen and for the described equation, the ratio of O/C should be less than 0.667 (Al-Zareer et al., 2018a).

3.2. Major system components

The analysis is conducted on the major system components to investigate the system performance and the effect on the system performance. All the subscripts used in the balance equations refers to the Aspen plus illustration shown in Fig. 2. In the balance equations of the major components, the model equations are only described once even if same component exists multiple time in the flowsheet and the stream numbers are defined on the basis of the very first component in the flowsheet. The equations used during the analysis of major components are arranged below:

Yield reactor

$$\dot{m}_{s1}LHV_{s1} + \dot{Q}_{Decomp} = \dot{m}_{s2}LHV_{s2} \tag{5}$$

$$\dot{m}_{s1}ex_{s1} + \dot{E}x_{\dot{Q}_{Decomp}} = \dot{m}_{s2}ex_{s2} + \dot{E}x_d \tag{6}$$

Gasification reactor

$$\dot{m}_{s2}LHV_{s2} + \dot{m}_{s3}h_{s3} + \dot{m}_{s19}h_{s19} - \dot{Q}_{Decomp} = \dot{m}_{s20}h_{s20} \tag{7}$$

$$\dot{m}_{s2}ex_{s2} + \dot{m}_{s3}ex_{s3} + \dot{m}_{s19}ex_{s19} - \dot{E}x_{\dot{Q}_{Decomp}} = \dot{m}_{s20}ex_{s20} + \dot{E}x_d \tag{8}$$

Compressor

$$\dot{m}_{s5}h_{s5} + \dot{W}_{in} = \dot{m}_{s6}h_{s6} \tag{9}$$

$$\dot{m}_{s5}ex_{s5} + \dot{W}_{in} = \dot{m}_{s6}ex_{s6} + \dot{E}x_d \tag{10}$$

Distillation column

$$\dot{m}_{s8}h_{s8} + \dot{Q}_{RB} = \dot{m}_{s9}h_{s9} + \dot{m}_{s11}h_{s11} + \dot{Q}_{RC} \tag{11}$$

$$\dot{m}_{s8}ex_{s8} + \dot{E}x_{\dot{Q}_{in}} = \dot{m}_{s9}ex_{s9} + \dot{E}x_d + \dot{m}_{s11}ex_{s11} + \dot{E}x_{\dot{Q}_{in}} \tag{12}$$

Turbine

$$\dot{m}_{s13}h_{s13} = \dot{m}_{s14}h_{s14} + \dot{W}_{out} \tag{13}$$

$$\dot{m}_{s13}ex_{s13} = \dot{m}_{s14}ex_{s14} + \dot{W}_{out} + \dot{E}x_d \tag{14}$$

Pump

$$\dot{m}_{s29}h_{s29} + \dot{W}_{in} = \dot{m}_{s22}h_{s22} \tag{15}$$

$$\dot{m}_{s29}ex_{s29} + \dot{W}_{in} = \dot{m}_{s22}ex_{s22} + \dot{E}x_d \tag{16}$$

WGSR

$$\dot{m}_{s30}h_{s30} = \dot{m}_{s33}h_{s33} + \dot{Q}_{out} \tag{17}$$

$$\dot{m}_{s30}ex_{s30} = \dot{m}_{s33}ex_{s33} + \dot{E}x_{\dot{Q}_{out}} + \dot{E}x_d \tag{18}$$

Combustion reactor

$$\dot{m}_{s34}h_{s34} + \dot{m}_{s39}h_{s39} = \dot{m}_{s40}h_{s40} + \dot{Q}_{out} \tag{19}$$

$$\dot{m}_{s34}ex_{s34} + \dot{m}_{s39}ex_{s39} = \dot{m}_{s40}ex_{s40} + \dot{E}x_{\dot{Q}_{out}} + \dot{E}x_d \tag{20}$$

Separator

$$\dot{m}_{s33}h_{s33} = \dot{m}_{s34}h_{s34} + \dot{m}_{s35}h_{s35} \tag{21}$$

$$\dot{m}_{s33}ex_{s33} = \dot{m}_{s34}ex_{s34} + \dot{m}_{s35}ex_{s35} + \dot{E}x_d \tag{22}$$

Heat Exchanger

$$\dot{m}_{s6}h_{s6} + \dot{m}_{s10}h_{s10} + \dot{m}_{s12}h_{s12} = \dot{m}_{s7}h_{s7} + \dot{m}_{s13}h_{s13} + \dot{m}_{s17}h_{s17} \tag{23}$$

$$\dot{m}_{s6}ex_{s6} + \dot{m}_{s10}ex_{s10} + \dot{m}_{s12}ex_{s12} = \dot{m}_{s7}ex_{s7} + \dot{m}_{s13}ex_{s13} + \dot{m}_{s17}ex_{s17} + \dot{E}x_d \tag{24}$$

Condenser

$$\dot{m}_{s27}h_{s27} = \dot{m}_{s29}h_{s29} + \dot{Q}_{out} \tag{25}$$

$$\dot{m}_{s27}ex_{s27} = \dot{m}_{s29}ex_{s29} + \dot{E}x_{\dot{Q}_{out}} + \dot{E}x_d \tag{26}$$

3.3. PEM electrolyzer

The PEM electrolyzer employed with the energy system is powered by the electricity produced by the steam Rankine cycle. It consumes electricity in order to split water into oxygen and hydrogen according to the following reactions which describe the energy required by the electrolyzer.

$$H_2O + \Delta H \rightarrow H_2 + \frac{1}{2}O_2 \tag{27}$$

$$\Delta H = \Delta G + T\Delta S \tag{28}$$

In the described equation, ΔH denotes the reaction enthalpy change, ΔG symbolizes Gibbs function and $T\Delta S$ characterizes thermal energy.

The hydrogen production rate carried out by the PEM the electrolyzer can be determined by the correlation:

$$\dot{N}_{H_2} = \frac{J_{el}}{2F} \tag{29}$$

Here, J_{el} is current density and F symbolizes Faraday's constant.

The power generated by the steam Rankine cycle is utilized as the electricity input for the electrolyzer.

$$\dot{W}_{PEM} = J_{el}V \tag{30}$$

$$V = V_0 + V_{act,a} + V_{act,c} + V_{con,a} + V_{con,c} + V_{Ohmic} \tag{31}$$

Here, V denotes voltage, and V_0 denotes for reversible cell potential. The Nernst equation is used to calculate the reversible cell potential where p represents partial pressure.

$$V_0 = \frac{\Delta G}{nF} + \frac{RT}{nF}\ln\left(\frac{(p_{H_2})\,(p_{O_2})^{0.5}}{p_{H_2O}}\right) \tag{32}$$

In the PEM electrolyzer, the correlations used to calculate activation over-potential at cathode and anode are described in Eqs. ((31) and (32)) and equations used to calculate the exchange current density are arranged as follows (Briguglio and Antonucci, 2015):

$$J_{o,c} = J_c^{ref}\exp\left(\frac{E_{act,c}}{RT}\right) \tag{33}$$

$$J_{o,a} = J_a^{ref}\exp\left(\frac{E_{act,a}}{RT}\right) \tag{34}$$

$$V_{act,c} = \left(\frac{RT}{F}\right)sinh^{-1}\left(\frac{J_{el}}{2J_{o,c}}\right) \tag{35}$$

$$V_{act,a} = \left(\frac{RT}{F}\right)sinh^{-1}\left(\frac{J_{el}}{2J_{o,a}}\right) \tag{36}$$

Here, J^{ref} indicates the pre-exponential factor and the ohmic over-potential is given by:

$$V_{Ohmic} = R_{PEM}J_{el} \tag{37}$$

3.4. Overall system efficiencies

The heat input source for the designed system is the biomass gasification and the major subsystems are entrained flow gasifier, CAS unit, double-stage Rankine cycle, WGSR, gas–steam combined cycle and PEM electrolyzer. The overall energy and exergy efficiency equations for the designed system are described as Eqs. (38) and (39) given in Box I .

4. Results and discussion

Both energy and exergy analyses of the biomass integrated energy system are conducted and during the performance investigation, parameters like biomass flow rate, steam flow rate, air input flow rate, combustion reactor temperature, and power supplied to the electrolyzer are varied to explore the system performance. The state point properties of each stream in the simulation design are arranged in a Table 3. The results concluded by the designed energy system including overall system efficiencies, electrical power output, heating and hydrogen production are arranged in Table 4. The modeled integrated system has numerous subsystems and the major commodities of the energy system are electricity, heating and hydrogen.

4.1. Effect of air input flow rate on the flow rates of different components in syngas

The significance of these sensitivity studies is to investigate the effect of input parameters on the biomass gasification and syngas. The key input of the entrained flow gasifier are steam, oxygen and biomass. This section investigates the effect of these input parameters on the syngas gas composition and flow rate of each specie. These sensitivity studies can help to scale up the designed system and can also be comprehended further to achieve the plant scale results. Each figure displays the deviation in the syngas composition with different input flow rates. Fig. 3 exhibits the effect of input air flow rate entering through the CAS unit on the hydrogen flow rate in the syngas at different intervals of the steam mass flow rate entering to the entrained flow gasifier. The input air flow rate is varied from 0 to 6 kg/s at different intervals of the steam flow rate from 1 to 5 kg/s and its effect on the hydrogen flow rate is drawn on the graphical representation. The pattern of the figure shows that in the beginning, with the rise in input air flow rate, the hydrogen production rate decrease rapidly up to the air flow rate of almost 2 kg/s and then it becomes almost zero for the cases of higher steam flow rates while for lower

$$\eta_{ov} = \frac{\dot{m}_{S37(H_2)}LHV_{H_2} + \dot{m}_{elect(H_2)}LHV_{H_2} + \dot{Q}_{Heating} + \dot{W}_{B10} + \dot{W}_{B14} + \dot{W}_{B16} + \dot{W}_{B17} + \dot{W}_{B26} + \dot{W}_{B29} - (\dot{W}_{B4} + \dot{W}_{B12} + \dot{W}_{B19} + \dot{W}_{B31} + \dot{W}_{elect})}{\dot{m}_{biomass}LHV_{biomass} + \dot{W}_{RFG,CAS}} \quad (38)$$

$$\psi_{ov} = \frac{\dot{m}_{S37(H_2)}ex_{H_2} + \dot{m}_{elect(H_2)}ex_{H_2} + \dot{E}x_{Q_{Heating}} + \dot{W}_{B10} + \dot{W}_{B14} + \dot{W}_{B16} + \dot{W}_{B17} + \dot{W}_{B26} + \dot{W}_{B29} - (\dot{W}_{B4} + \dot{W}_{B12} + \dot{W}_{B19} + \dot{W}_{B31} + \dot{W}_{elect})}{\dot{m}_{biomass}ex_{biomass} + \dot{W}_{RFG,CAS}} \quad (39)$$

Box I.

Table 3
State point data of the designed energy system.

State no.	Temperature (°C)	Pressure (kPa)	Mass vapor fraction	Mass liquid fraction	Mass solid fraction	Mass enthalpy (kJ/kg)	Mass flow (kg/s)
S1	25.0	2431.8	0.0	0.0	1.0	11 220.9	0.4
S2	850.0	101.3	0.4	0.0	0.6	1514.4	0.4
S3	423.5	2431.8	1.0	0.0	0.0	−12 677.3	2.9
S5	41.9	101.3	1.0	0.0	0.0	16.8	11.1
S6	386.0	810.6	1.0	0.0	0.0	373.7	11.1
S7	−145.6	810.6	1.0	0.0	0.0	−181.4	11.1
S8	−149.0	506.6	1.0	0.0	0.0	−181.4	11.1
S9	−178.8	506.6	0.0	1.0	0.0	−398.9	8.4
S10	−191.8	152.0	0.1	0.9	0.0	−398.9	8.4
S11	−165.1	506.6	0.0	1.0	0.0	−375.7	2.8
S12	−179.5	152.0	0.1	0.9	0.0	−375.7	2.8
S13	231.1	152.0	1.0	0.0	0.0	215.4	8.4
S14	200.7	111.5	1.0	0.0	0.0	183.4	8.4
S15	30.0	111.5	1.0	0.0	0.0	5.0	8.4
S17	25.0	152.0	1.0	0.0	0.0	−0.4	2.8
S19	483.8	2431.8	1.0	0.0	0.0	451.3	2.8
S20	1513.0	2431.8	1.0	0.0	0.0	−5119.4	6.1
S21	1397.4	1440.0	1.0	0.0	0.0	−5349.5	6.1
S22	31.5	5000.0	0.0	1.0	0.0	−16 008.0	2.5
S23	651.2	5000.0	1.0	0.0	0.0	−12 191.0	2.5
S25	381.7	500.0	1.0	0.0	0.0	−12 736.6	2.5
S27	90.6	10.0	1.0	0.0	0.0	−13 300.4	2.5
S29	30.0	10.0	0.0	1.0	0.0	−16 020.4	2.5
S30	530.0	1440.0	1.0	0.0	0.0	−6926.9	6.1
S33	450.0	1440.0	1.0	0.0	0.0	−7057.0	6.1
S34	450.0	1440.0	1.0	0.0	0.0	−7057.1	6.1
S35	450.0	1440.0	1.0	0.0	0.0	6179.2	0.0
S37	25.0	100.0	1.0	0.0	0.0	0.6	0.0
S38	26.0	100.0	1.0	0.0	0.0	0.8	0.1
S39	596.3	2300.0	1.0	0.0	0.0	607.4	0.1
S40	500.0	2300.0	1.0	0.0	0.0	−6882.6	6.1
S42	222.3	122.0	1.0	0.0	0.0	−7299.9	6.1
S43	465.5	122.0	1.0	0.0	0.0	−6927.6	6.1
S44	50.0	122.0	0.5	0.5	0.0	−8767.3	6.1
S45	462.7	1000.0	1.0	0.0	0.0	−12 572.9	3.3
S47	104.8	10.0	1.0	0.0	0.0	−13 273.6	3.3
S49	25.0	10.0	0.0	1.0	0.0	−16 044.6	3.3
S50	25.2	1000.0	0.0	1.0	0.0	−16 042.4	3.3

steam flow rates of 1 and 2 kg/s, it decreases gradually. The lines with the different colors and different markers are used in order to differentiate according to the legends. The effect of input air flow rate is plotted against the carbon dioxide flow rate in Fig. 4. It represents that with the increase in input air flow rate, the flow rate of carbon dioxide is effected at different steam flow rates. The range considered for input air flow rate is 0 to 6 kg/s and its effect on carbon dioxide flow rate is observed at fixed steam flow rate from 1 to 5 kg/s. The graphical representation shows that with the increase in the air input flow rate, the flow rate of carbon dioxide increases simultaneously till the input air flow rate of around 1.5 kg/s and after this point, additional air behaves like excess air and it does not affect the flow rate of carbon dioxide for the cases of higher steam flow rates while for lower steam flow rates of 1 and 2 kg/s, it increases gradually. The different flow rate of steam are represented with the different colored lines and markers in the graph as well as their legends.

In Fig. 5, the influence of air input flow rate is drawn against the flow rate of carbon monoxide. To observe this effect, some ranges of the steam flow rate are specified. For example, in each case, the input air flow rate varies from 1 to 6 kg/s by setting the steam flow rate at fixed points from 1 to 5 kg/s and its effect is observed on the carbon monoxide flow rate. It can be seen that with the rise in air input flow rate, the flow rate of carbon monoxide decreases rapidly till the air input flow rate of around 1.8 kg/s and once it crosses this limit, the carbon monoxide flow rate becomes zero for the cases of higher steam flow rates while for lower steam flow rates, it decreases gradually.

Fig. 6 shows the effects of air input flow rate on the steam flow rate in the output of entrained flow gasifier at the fixed intervals of the input air flow rate. The range considered for the input air

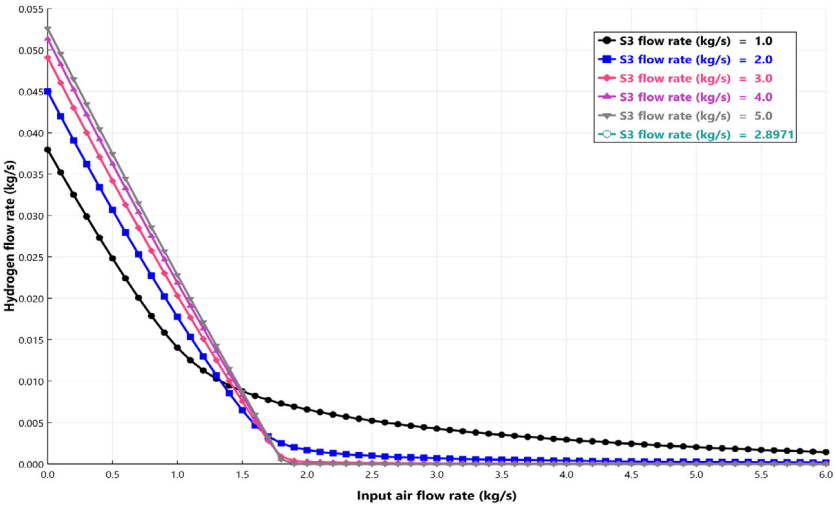

Fig. 3. Effect of input air flow rate on H_2 flow rate in syngas with change in steam flow rate.

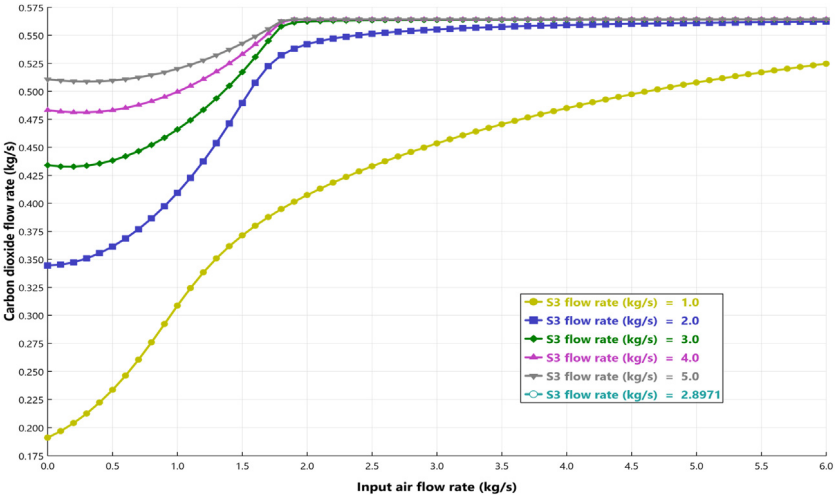

Fig. 4. Effect of input air flow rate on CO_2 flow rate in syngas with change in steam flow rate.

flow rate is from 1 to 6 kg/s and the different intervals of the input steam flow rate are taken from 1 to 5 kg/s. The different input steam from rates from 1 to 5 kg/s is represented with the different colors. The plot shows that with the increase in air flow rate, the steam flow rate in the output of the gasifier increases in the beginning up-to some point and then it becomes constant and does not get affected by increase in air flow rate.

The influence of the input air flow rate is plotted against the oxygen flow rate in the output of the gasifier in Fig. 7. The range of the input air flow is taken from 1 to 10 kg/s and the steam input flow rate is taken for the intervals of 1 to 5 kg/s. The markers with different colors are selected for different ranges of the steam flow rate. In the start, the flow rate of oxygen remains constant because the reaction itself has oxygen requirement. Thus, once the oxygen flow rate reaches to the required flow rate, it increases rapidly for the cases of higher steam flow rates while for lower steam flow rates of 1 and 2 kg/s, it increases progressively.

4.2. Effect of combustion reactor temperature on the Brayton cycle turbine power, steam Rankine cycle turbine power and the Rankine cycle turbine input temperature

The significance of this sensitivity study is to investigate the effect of combustion reactor temperature on the Brayton cycle turbine power, steam Rankine cycle turbine power and the Rankine cycle turbine input temperature. The range of temperature considered for the parametric study is 400 to 600 °C. It can be observed that with the rise in combustion reactor temperature, the Brayton cycle turbine power increases from 2209 to 2937 kW, steam Rankine cycle turbine power rises from 2240 to 2539 kW and the Rankine cycle turbine input temperature increases from 370 to 557 °C. The combustion reactor temperature is plotted against the Brayton cycle turbine power, steam Rankine cycle turbine power and the Rankine cycle turbine input

Table 4
The summary of the results obtained for the integrated system.

Block name	Component	Result
	Overall energy efficiency of the system	53.72%
	Overall exergy efficiency of the system	45.5%
B10	Turbine power	0.27 MW
B14	Turbine power	1.39 MW
B18	Heating	479 kW
B16	High-pressure turbine power	1.36 MW
B17	Low-pressure turbine power	1.41 MW
B21	Heat recovery from WGSR	0.79 MW
B26	Brayton cycle turbine power	2.56 MW
B29	Steam Rankine cycle turbine power	2.28 MW
PEM electrolyzer	Hydrogen production	10.74 mol/s

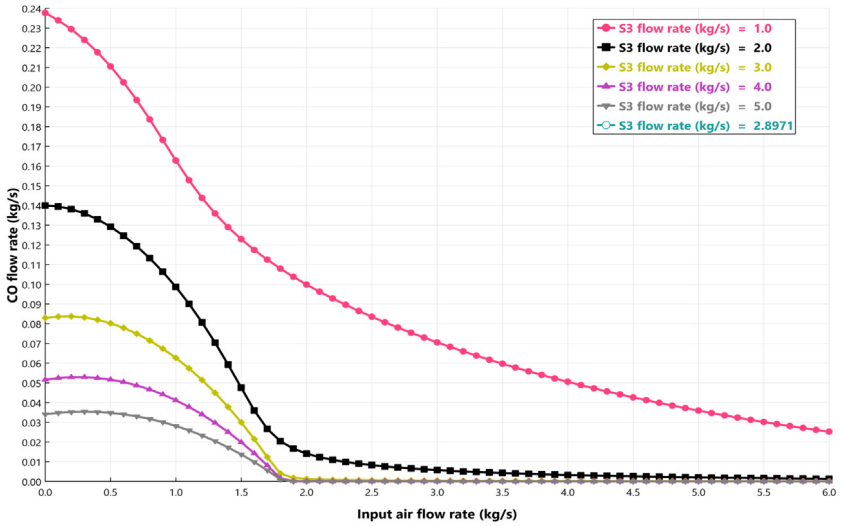

Fig. 5. Influence of input air flow rate on CO flow rate in syngas with change in steam flow rate.

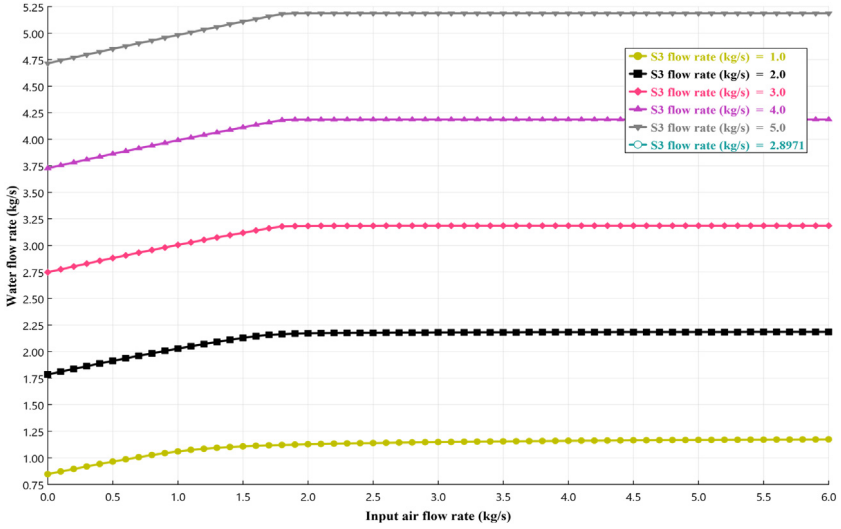

Fig. 6. Effect of air flow rate on H_2O flow rate at different intervals of steam input flow rate.

temperature in Fig. 8. Three different colored lines are used to differentiate three different parameters and arranged in the legends as well. Fig. 8 shows that with the rise in the combustion reaction temperature, the power generated by the Brayton cycle turbine increases and this increase results into increased temperature at the steam Rankine cycle turbine inlet and the increased temperature generates more power in the steam turbine.

4.3. Effect of combustion reactor temperature on the hydrogen production rate and steam turbine power

Fig. 9 exhibits the effect of the combustion reaction temperature on the steam Rankine cycle turbine power and the hydrogen production rate. The range of the temperature considered for the parametric investigation is 400 to 600 °C. As it has been concluded from Fig. 7 that combustion reactor temperature increases the steam turbine power, the system is designed in a way that the power produced by the steam Rankine cycle is employed to the PEM electrolyzer. Thus, this power directly affects the hydrogen production rate. It can be seen that with the rise in combustion reaction temperature, the steam turbine power increases with results in the increased hydrogen production.

4.4. Effect of power consumed by PEM electrolyzer on hydrogen production rate and exergy destruction rate of PEM electrolyzer

The effect of the electrical power employed to the PEM electrolyzer is investigated against the hydrogen production rate and exergy destruction of the PEM electrolyzer. The orange line in the plot represents the hydrogen production rate while the dark blue line gives the exergy destruction rate. For considering the steam turbine power range, some parametric studies have already conduction so the range taken for the PEM electrolyzer input power is from 2000 to 2500 kW. The graphical representation shows that with the rise in the power supplied to the PEM electrolyzer, both hydrogen production rate and the exergy destruction rate

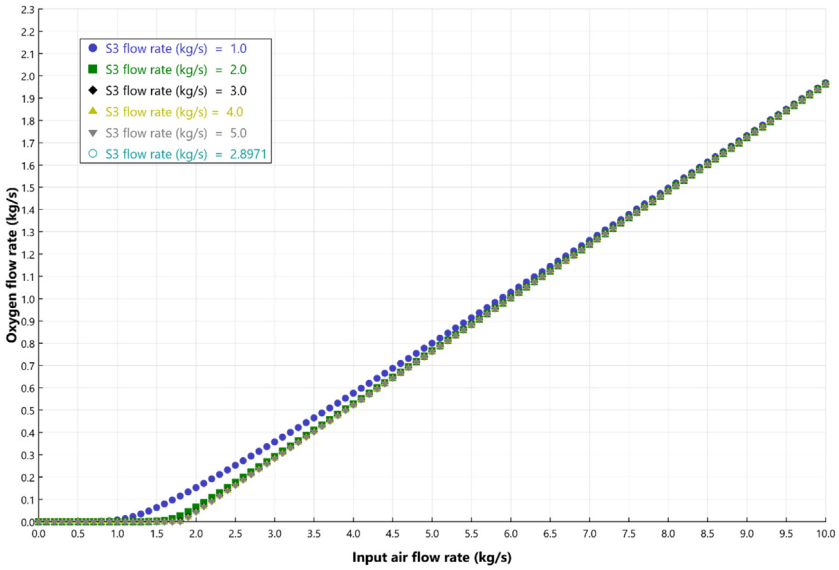

Fig. 7. The influence of air flow rate on O_2 flow rate in syngas with change in steam flow rate.

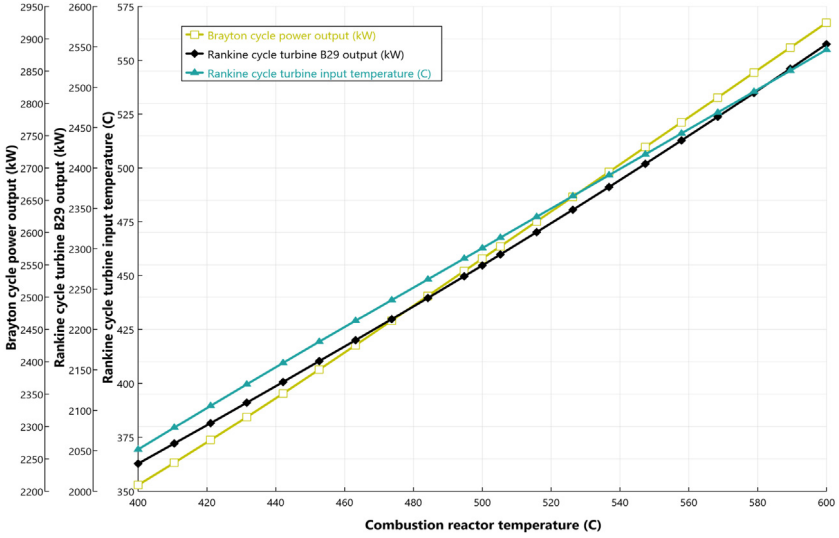

Fig. 8. Combustion temperature effect on gas and steam Rankine cycle and Rankine cycle input temperature.

increases. Fig. 11 exhibits the overall power distribution in the proposed system. The legends are representing each block with respect to the specific section in the pie chart (see Fig. 10).

4.5. Validation

The results obtained by the proposed system are validated using different studies considering the gasification. At some points, the subsystems are needed to be validated as this paper presents a new configuration. Al-Zareer et al. (2018a) conducted the multi-objective optimization of a gasification based integrated system and proposed the energy efficiency in the range of 39.1% to 56.6% and exergy efficiency of 60.2%. Al-Zareer et al. (2018b) published another study on multigeneration system using cryogenic air separation unit utilizing distillation column and found the energetic and exergetic efficiencies of 51.3% and 47.6% while this proposed study concludes the energy efficiency of 53.7% and exergy efficiency of 45.5%, respectively.

5. Conclusions

A novel energy system based on biomass gasification is modeling and performance investigation is conducted for the system. The integrated system is designed to produce the useful commodities of electricity, heating and hydrogen. The novel configuration resulted into some emerging outcomes in terms of multigeneration capability with high efficiency rates. The cryogenic air separation unit is integrated with the system to provide with the required amount of oxygen. Aspen plus and EES software tools are used for system simulation and modeling. Multiple parametric investigations are conducted on the basis of different parameters, such as input air flow rate, biomass flow rate, steam flow rate, combustion reactor temperature, and power supplied to the electrolyzer. The electrical power output of the designed energy system is 1.4 MW for the biomass flow rate of 0.4 kg/s. The hydrogen production rate of the designed biomass based integrated system is 10.74 mol/s. The pilot scale implementation of the proposed system is recommended for future studies. The energy and exergy efficiencies of the overall energy system are obtained to be 53.7% and 45.5% respectively.

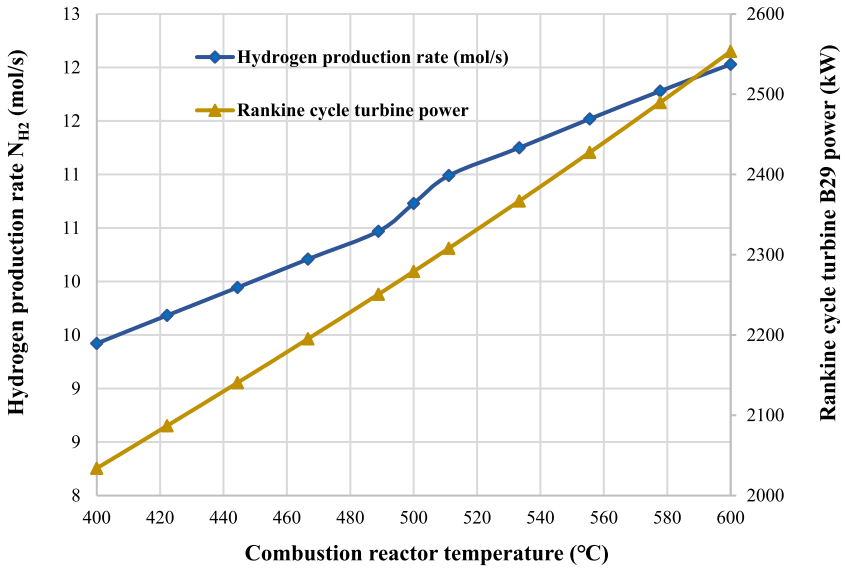

Fig. 9. Variation in hydrogen production rate and steam Rankine cycle power with the change in combustion reactor temperature.

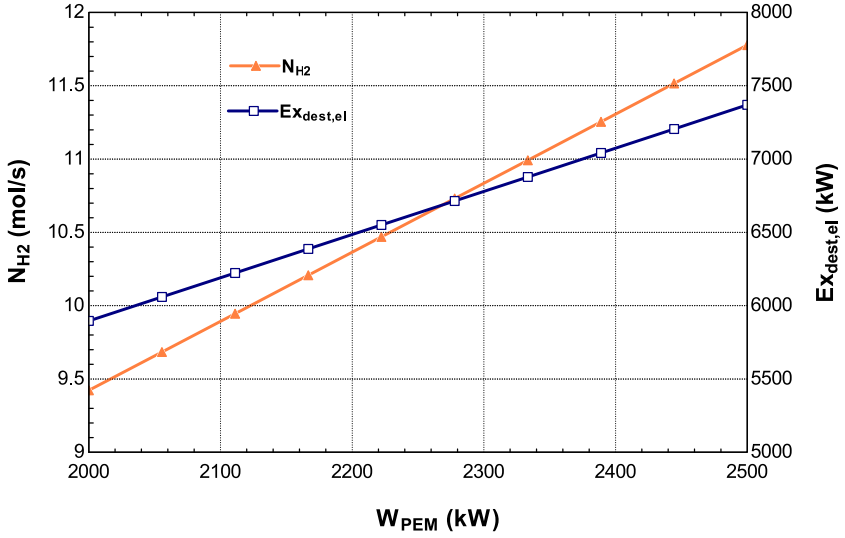

Fig. 10. Electrolyzer input power effect on hydrogen production and exergy destruction.

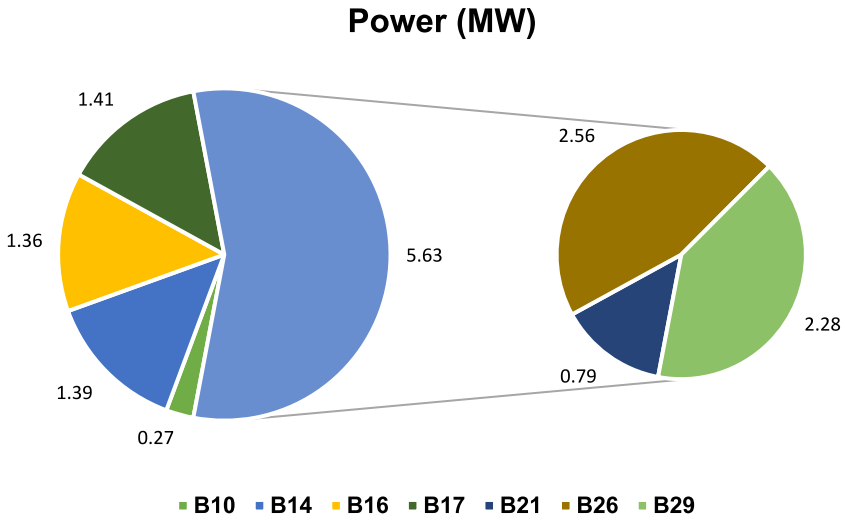

Fig. 11. Power distribution in the integrated system.

Nomenclature

A	Area (m^2)
$\dot{E}n$	Energy rate (kW)
ex	Specific exergy (kJ/kg)
h	Specific enthalpy (kJ/kg)
F	Faraday's constan
LHV	Lower heating value (kJ/kg)
HHV	Higher heating value (kJ/kg)
J	Current density A/m2)
k	Thermal conductivity (W/m2K)
$\dot{m}$	Mass flow rate (kg/s)
$\dot{Q}$	Heat rate (kW)
s	Specific entropy (kJ/kg K)
$\dot{N}$	Number of moles
$\dot{S}_{gen}$	Entropy generation rate (kW/K)
T	Temperature (°C)
V_{Ohmic}	Ohmic over potential (V)
$\dot{W}$	Power or work rate (kW)
Greek letters	
η	Energy efficiency
ψ	Exergy efficiency
Subscripts	
0	Reference conditions
Comp	Compressor
ch	Chemical
en	Energy
elect	Electrolyzer
ex	Exergy
i	Input
ov	Overall
ph	Physical
W	Work
Acronyms	
CAS	Cryogenic Air Separation
EES	Engineering Equation Solver
HEX	Heat Exchanger
HPT	High Pressure Turbine
LPT	Low Pressure Turbine
PEM	Proton Exchanger Membrane
WGSR	Water Gas Shift Reactor

Declaration of competing interest

The authors declare that they have no known competing financial interests or personal relationships that could have appeared to influence the work reported in this paper.

CRediT authorship contribution statement

H. Ishaq: Conceived and designed the analysis, Collected the data, Contributed data or analysis tools, Performed the analysis, Wrote the paper. **I. Dincer:** Project management, Data validation, Review & editing, Supervision.

References

Abuadala, A., Dincer, I., Naterer, G.F., 2009. Exergy analysis of hydrogen production from biomass gasification. Int. J. Hydrog. Energy 35, 4981–4990.

Al-Zareer, M., Dincer, I., Rosen, M.A., 2018a. Multi-objective optimization of an integrated gasification combined cycle for hydrogen and electricity production. Comput. Chem. Eng. 117, 256–267.

Al-Zareer, M., Dincer, I., Rosen, M.A., 2018b. Analysis and assessment of a hydrogen production plant consisting of coal gasification, thermochemical water decomposition and hydrogen compression systems. Energy Convers. Manag. 157, 600–618.

Andersson, J., Lundgren, J., 2014. Techno-economic analysis of ammonia production via integrated biomass gasification. Appl. Energy 130, 484–490.

Atif, M., Al-Sulaiman, F.A., 2018. Energy and exergy analyses of recompression brayton cycles integrated with a solar power tower through a two-tank thermal storage system. J. Energy Eng. 144.

Augustine, A.S., Ma, Y.H., Kazantzis, N.K., 2011. High pressure palladium membrane reactor for the high temperature water-gas shift reaction. Int. J. Hydrog. Energy 36, 5350–5360.

Basu, P., Francisco, S., 2010. Biomass gasification design handbook. Biomass Gasif. Pyrolysis 45, 117–165.

Briguglio, N., Antonucci, V., 2015. Overview of PEM electrolysis for hydrogen production. PEM Electrolysis Hydrog. Prod. Princ. Appl. 389. http://dx.doi.org/10.1201/b19096-2.

Carmo, M., Fritz, D.L., Mergel, J., Stolten, D., 2013. A comprehensive review on PEM water electrolysis. Int. J. Hydrog. Energy 38, 4901–4934.

Cengel, Y.A., Boles, M.A., 2015. Thermodynamics: An Engineering Approach 8th Edition. McGraw-Hill, http://dx.doi.org/10.1017/CBO9781107415324.004.

Dimpl, E., 2011. Small-scale electricity generation from biomass part I: Biomass gasification. Fed. Minist. Econ. Corp. Dev..

Ellis, N., Masnadi, M.S., Roberts, D.G., Kochanek, M.A., Ilyushechkin, A.Y., 2015. Mineral matter interactions during co-pyrolysis of coal and biomass and their impact on intrinsic char co-gasification reactivity. Chem. Eng. J. 279, 402–408.

Gunarathne, D.S., Mellin, P., Yang, W., Pettersson, M., Ljunggren, R., 2016. Performance of an effectively integrated biomass multi-stage gasification system and a steel industry heat treatment furnace. Appl. Energy 170, 353–361.

Ishaq, H., Dincer, I., 2019. A comparative evaluation of OTEC, solar and wind energy based systems for clean hydrogen production. J. Clean Prod. 118736. http://dx.doi.org/10.1016/j.jclepro.2019.118736.

Islam, S., Dincer, I., Yilbas, B.S., 2017. Analysis and assessment of a biomass energy-based multigeneration system with thermoelectric generators. Energy Fuels 156, 746–756.

Khalid, F., Dincer, I., Rosen, M.A., 2015. Energy and exergy analyses of a solar-biomass integrated cycle for multigeneration. Sol. Energy 112, 290–299.

Muradov, N.Z., Veziroğlu, T.N., 2008. 'Green' path from fossil-based to hydrogen economy: An overview of carbon-neutral technologies. Int. J. Hydrog, Energy 33, 6804–6839.

Ozturk, M., 2017. Energy and exergy analysis of renewable energy sources based integrated system for multi-generation application. Int. J. Exergy 22, 1. http://dx.doi.org/10.1504/ijex.2017.10003719.

Roddy, D.J., Manson-Whitton, C., 2012. Biomass gasification and pyrolysis. Compr. Renew. Energy 5, 133–153.

Safari, F., Tavasoli, A., Ataei, A., 2016. Gasification of sugarcane bagasse in supercritical water media for combined hydrogen and power production: a novel approach. Int. J. Environ. Sci. Technol. 13, 2393–2400.

Sikarwar, V.S., Zhao, M., Clough, P., Yao, J., Zhong, X., Memon, M.Z., Shah, N., Anthony, E.J., Fennell, P.S., 2016. An overview of advances in biomass gasification. Energy Environ. Sci. 9, 2939–2977.

Turner, J., Sverdrup, G., Mann, M.K., Maness, P.C., Kroposki, B., Ghirardi, M., Evans, R.J., Blake, D., 2008. Renewable hydrogen production. Int. J. Energy Res. 32, 379–407.

Uzi, A., Shen, Y., Kawi, S., Levy, A., Wang, C.H., 2019. Permittivity and chemical characterization of woody biomass during pyrolysis and gasification. Chem. Eng. J. 355, 255–268.

Van der Ham, L.V., Kjelstrup, S., 2010. Exergy analysis of two cryogenic air separation processes. Energy 35, 4731–4739.

Yan, L., Yue, G., He, B., 2015. Exergy analysis of a coal/biomass co-hydrogasification based chemical looping power generation system. Energy 93, 1778–1787.